7. H. S. Chung, K. McHale, J. M. Louis, W. A. Eaton, *Science* **335**, 981–984 (2012).
8. H. S. Chung, W. A. Eaton, *Nature* **502**, 685–688 (2013).
9. G. Hummer, *J. Chem. Phys.* **120**, 516–523 (2004).
10. H. S. Chung, J. M. Louis, W. A. Eaton, *Proc. Natl. Acad. Sci. U.S. A.* **106**, 11837–11844 (2009).
11. H. S. Chung, I. V. Gopich, *Phys. Chem. Chem. Phys.* **16**, 18644–18657 (2014).
12. D. E. Shaw *et al.*, in *SC'09, Proceedings of the Conference on High Performance Computing, Networking, Storage, and Analysis*, Portland, OR, 14 to 20 November 2009 (ACM Press, New York, 2009); http://dl.acm.org/citation.cfm?id=1654099.
13. K. Lindorff-Larsen, S. Piana, R. O. Dror, D. E. Shaw, *Science* **334**, 517–520 (2011).
14. S. Piana, K. Lindorff-Larsen, D. E. Shaw, *Biophys. J.* **100**, L47–L49 (2011).
15. S. Piana, K. Lindorff-Larsen, D. E. Shaw, *Proc. Natl. Acad. Sci. U.S.A.* **109**, 17845–17850 (2012).
16. D. E. Shaw *et al.*, *Science* **330**, 341–346 (2010).
17. R. B. Best, G. Hummer, W. A. Eaton, *Proc. Natl. Acad. Sci. U.S.A.* **110**, 17874–17879 (2013).
18. S. J. Hagen, J. Hofrichter, A. Szabo, W. A. Eaton, *Proc. Natl. Acad. Sci. U.S.A.* **93**, 11615–11617 (1996).
19. J. Kubelka, J. Hofrichter, W. A. Eaton, *Curr. Opin. Struct. Biol.* **14**, 76–88 (2004).
20. S. T. R. Walsh, H. Cheng, J. W. Bryson, H. Roder, W. F. DeGrado, *Proc. Natl. Acad. Sci. U.S.A.* **96**, 5486–5491 (1999).
21. Y. Zhu *et al.*, *Proc. Natl. Acad. Sci. U.S.A.* **100**, 15486–15491 (2003).
22. D. U. Ferreiro, E. A. Komives, P. G. Wolynes, *Q. Rev. Biophys.* **47**, 285–363 (2014).
23. H. S. Chung *et al.*, *J. Phys. Chem. A* **115**, 3642–3656 (2011).
24. I. V. Gopich, A. Szabo, *J. Phys. Chem. B* **111**, 12925–12932 (2007).
25. I. V. Gopich, A. Szabo, *J. Phys. Chem. B* **113**, 10965–10973 (2009).
26. A. Ansari, C. M. Jones, E. R. Henry, J. Hofrichter, W. A. Eaton, *Science* **256**, 1796–1798 (1992).
27. D. E. Sagnella, J. E. Straub, D. Thirumalai, *J. Chem. Phys.* **113**, 7702–7711 (2000).
28. H. S. Chung, T. Cellmer, J. M. Louis, W. A. Eaton, *Chem. Phys.* **422**, 229–237 (2013).
29. Materials and methods are available as supplementary materials on *Science* Online.
30. J. C. F. Schulz, L. Schmidt, R. B. Best, J. Dzubiella, R. R. Netz, *J. Am. Chem. Soc.* **134**, 6273–6279 (2012).
31. G. S. Jas, W. A. Eaton, J. Hofrichter, *J. Phys. Chem. B* **105**, 261–272 (2001).
32. T. Cellmer, E. R. Henry, J. Hofrichter, W. A. Eaton, *Proc. Natl. Acad. Sci. U.S.A.* **105**, 18320–18325 (2008).
33. B. G. Wensley *et al.*, *Nature* **463**, 685–688 (2010).
34. B. G. Wensley, L. G. Kwa, S. L. Shammas, J. M. Rogers, J. Clarke, *J. Mol. Biol.* **423**, 273–283 (2012).
35. B. G. Wensley *et al.*, *Proc. Natl. Acad. Sci. U.S.A.* **109**, 17795–17799 (2012).
36. A. Borgia *et al.*, *Nat. Commun.* **3**, 1195 (2012).
37. J. J. Portman, S. Takada, P. G. Wolynes, *J. Chem. Phys.* **114**, 5082–5096 (2001).
38. D. de Sancho, A. Sirur, R. B. Best, *Nat. Commun.* **5**, 4307 (2014).
39. W. Zheng, D. De Sancho, T. Hoppe, R. B. Best, *J. Am. Chem. Soc.* **137**, 3283–3290 (2015).
40. I. Echeverria, D. E. Makarov, G. A. Papoian, *J. Am. Chem. Soc.* **136**, 8708–8713 (2014).
41. G. Ciccotti, M. Ferrario, J. T. Hynes, R. Kapral, *J. Chem. Phys.* **93**, 7137–7147 (1990).
42. R. G. Mullen, J. E. Shea, B. Peters, *J. Chem. Theory Comput.* **10**, 659–667 (2014).
43. S. H. Northrup, J. T. Hynes, *J. Chem. Phys.* **73**, 2700–2714 (1980).

ACKNOWLEDGMENTS

We thank R. Best and A. Szabo for many helpful and insightful discussions. Work at NIH was supported by the Intramural Research Program of the NIDDK. We are also thank J. M. Louis for the preparation, dye labeling, and purification of the protein used in this work, with technical assistance from A. Aniana.

SUPPLEMENTARY MATERIALS

www.sciencemag.org/content/349/6255/1504/suppl/DC1
Materials and Methods
Figs. S1 to S14
Tables S1 to S8
References (*44*–*55*)

16 March 2015; accepted 13 August 2015
10.1126/science.aab1369

REPORTS

QUANTUM SIMULATION

Observation of chiral edge states with neutral fermions in synthetic Hall ribbons

M. Mancini,[1] G. Pagano,[1] G. Cappellini,[2] L. Livi,[2] M. Rider,[3,4] J. Catani,[5,2] C. Sias,[6,2] P. Zoller,[3,4] M. Inguscio,[6,1,2] M. Dalmonte,[3,4] L. Fallani[1,2]*

Chiral edge states are a hallmark of quantum Hall physics. In electronic systems, they appear as a macroscopic consequence of the cyclotron orbits induced by a magnetic field, which are naturally truncated at the physical boundary of the sample. Here we report on the experimental realization of chiral edge states in a ribbon geometry with an ultracold gas of neutral fermions subjected to an artificial gauge field. By imaging individual sites along a synthetic dimension, encoded in the nuclear spin of the atoms, we detect the existence of the edge states and observe the edge-cyclotron orbits induced during quench dynamics. The realization of fermionic chiral edge states opens the door for edge state interferometry and the study of non-Abelian anyons in atomic systems.

Ultracold atoms in optical lattices represent an ideal system for studying the physics of condensed matter problems in a fully tunable, controllable environment (*1*, *2*). One of the notable achievements in recent years has been the realization of synthetic background gauge fields, akin to magnetic fields in electronic systems. By exploiting light-matter interaction, it is possible to imprint a Peierls phase onto the atomic wave function. This phase is analogous to the Aharanov-Bohm phase experienced by a charged particle in a magnetic field (*3*–*5*). These gauge fields, first synthesized in Bose-Einstein condensates (*6*), have recently allowed for the realization of the Harper-Hofstadter Hamiltonian in ultracold bosonic two-dimensional (2D) lattice gases (*7*, *8*), whereas, following a complementary route based on accurate engineering of the single-particle Hamiltonian, Chern insulators have been also realized (*9*) in systems that lack a net magnetic field (*10*). These works are paving the way toward the investigation of different forms of bulk topological matter in atomic systems (*5*, *11*). In the present work, we are instead interested in the edge properties of fermionic systems under the effects of a synthetic gauge field. Fermionic edge states are a fundamental feature of 2D topological states of matter, such as quantum Hall and chiral spin liquids (*12*, *13*). Moreover, they are robust against changing the geometry of the system and can be observed even on Hall ribbons (*14*). In addition, fermionic edge states offer appealing prospects in quantum science, such as the realization of robust quantum information buses (*15*), and they are ideal starting points for the realization of non-Abelian anyons akin to Majorana fermions (*16*, *17*).

Here we report the observation of chiral edge states in a system of neutral fermions subjected to a synthetic magnetic field. We exploit the high level of control in our system to investigate the emergence of chirality as a function of the Hamiltonian couplings. These results have been enabled by an innovative approach, proposed in (*18*), where an internal (nuclear spin) degree of freedom of the atoms is used to encode a lattice structure lying in an "extra dimension" (*14*), providing direct access to edge physics. We synthesize a system of fermionic particles in an atomic Hall ribbon of tunable width pierced by an effective gauge field. One dimension is realized by an optical lattice, which induces a real tunneling t between different sites along direction $\hat{x}$ (Fig. 1A). The different internal spin states are coupled by a two-photon Raman transition, which provides a coherent controllable coupling $\Omega e^{i\varphi x}$ between different spin components. This can be interpreted as a complex tunneling amplitude between adjacent sites of an extra-dimensional lattice along a synthetic direction $\hat{m}$ (*14*, *19*). Furthermore, the phase imprinting laid out by the Raman beams amounts to the synthesis of an effective magnetic field for effectively charged particles (*4*) with flux $\varphi/2\pi$ (in units of the magnetic flux quantum)

[1]Department of Physics and Astronomy, University of Florence, I-50019 Sesto Fiorentino, Italy. [2]European Laboratory for Non-Linear Spectroscopy (LENS), I-50019 Sesto Fiorentino, Italy. [3]Institute for Quantum Optics and Quantum Information of the Austrian Academy of Sciences, A-6020 Innsbruck, Austria. [4]Institute for Theoretical Physics, University of Innsbruck, A-6020 Innsbruck, Austria. [5]Istituto Nazionale di Ottica del Consiglio Nazionale delle Ricerche (INO-CNR), Sezione di Sesto Fiorentino, I-50019 Sesto Fiorentino, Italy. [6]Istituto Nazionale di Ricerca Metrologica (INRIM), I-10135 Torino, Italy.
***Corresponding author. E-mail: fallani@lens.unifi.it**

per plaquette (*20*). The Hamiltonian describing the system is

$$H = \sum_j \sum_\alpha [-t(c^\dagger_{j,\alpha} c_{j+1,\alpha} + \text{h.c.}) + \mu_j n_{j,\alpha}] + \sum_j \sum_\alpha \left[\frac{\Omega_\alpha}{2}(e^{i\varphi j} c^\dagger_{j,\alpha} c_{j,\alpha+1} + \text{h.c.}) + \xi_\alpha n_{j,\alpha}\right] \quad (1)$$

where $c^\dagger_{j,\alpha}(c_{j,\alpha})$ are fermionic creation (annihilation) operators on the site (j,α) in the real (j) and synthetic (α = 1,2,3) dimensions, and $n_{j,\alpha} = c^\dagger_{j,\alpha} c_{j,\alpha}$. The first term describes the dynamics along $\hat{x}$, where t can be tuned by changing the intensity of the optical lattice beams. The dynamics along $\hat{m}$ is encoded in the second term: Ω_α can be controlled by changing the power of the Raman beams, whereas φ can be tuned by changing their angle (*20*). In Eq. 1, μ_j describes a weak trapping potential along $\hat{x}$, whereas ξ_α accounts for a state-dependent light shift, providing an energy offset along $\hat{m}$. h.c. stands for Hermitian conjugate. In our experiment, we produced large synthetic magnetic fields corresponding to $\varphi \simeq 0.37\pi$ per plaquette. For fermionic particles, we use alkaline-earth–like ^{173}Yb atoms, initially prepared in a degenerate Fermi gas. The sites of the synthetic dimension (Fig. 1B) are encoded in a subset of spin states $\{m\}$ out of the $I = 5/2$ nuclear spin manifold, thus providing fermionic "ladders" with up to six "legs." These atoms show SU(N)-invariant interactions [SU(N), special unitary group of degree N] (*21*), inhibiting the redistribution of the atoms among the different synthetic sites by collisional processes (*22*, *23*). The effect of these interactions—which is not fundamental for explaining the observations reported in this manuscript—has been taken into account in the theoretical model as a renormalization of the trap frequency (*20*). This is possible because the maximum filling fraction is $\eta \simeq 0.8$ atoms per site of the real-space lattice: For larger filling fractions commensurate with the lattice, possible insulating phases can be stabilized.

The key advantage offered by the implementation in a lattice that combines real and synthetic spaces is the possibility to work with a finite-sized system with sharp and addressable edges. Specifically, we focus on elementary configurations made up of fermionic ladders with a small number of legs connected by a tunnel coupling between them. A leg is constituted by a 1D chain of atoms trapped in the sites of the real lattice in a specific spin state, whereas the ladder "rungs" are provided by the synthetic tunneling (Fig. 1A). The number of legs can be set by controlling the light shifts ξ_α in such a way as to choose the number of spin states that are coupled by the Raman lasers (*20*).

We first consider the case of a two-leg ladder constituted by the nuclear spin states $m = -5/2$ and $m = -1/2$. A quantum degenerate ^{173}Yb Fermi gas with 1.6×10^4 atoms and an initial temperature $T \simeq 0.2T_F$ (where T_F is the Fermi temperature) is first spin-polarized in $m = -5/2$. By slowly turning on the intensity of the optical lattice along $\hat{x}$ (and of an additional strong lattice along $\hat{y}$ and $\hat{z}$ to suppress the dynamics along the other two real directions), we prepare a system of ladders in which all atoms occupy the $m = -5/2$ leg with less than one atom per site (i.e., in a conductive metallic state). Then, by controlling the intensity and frequency of the Raman beams (*20*), we slowly activate the tunnel

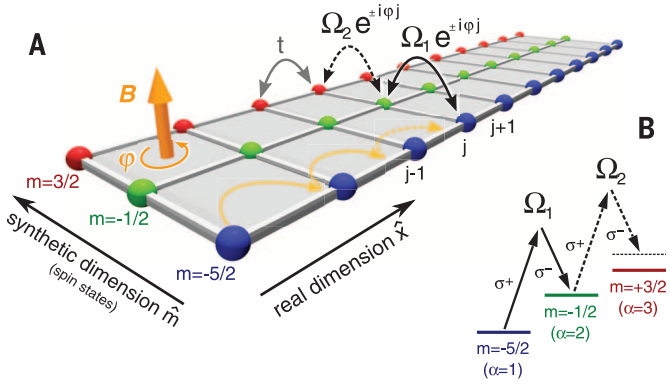

Fig. 1. A synthetic gauge field in a synthetic dimension. (**A**) We confine the motion of fermionic ultracold atoms in a hybrid lattice, generated by an optical lattice along a real direction $\hat{x}$ with tunneling t, and by laser-induced hopping between spin states along a synthetic direction $\hat{m}$. By inducing a complex tunneling $\Omega_{1,2}e^{i\varphi j}$ along $\hat{m}$, the atom wave function acquires a phase φ per plaquette, mimicking the effect of a transverse magnetic field **B** on effectively charged particles. (**B**) Scheme of the ^{173}Yb nuclear spin states and Raman transitions used in the experiment.

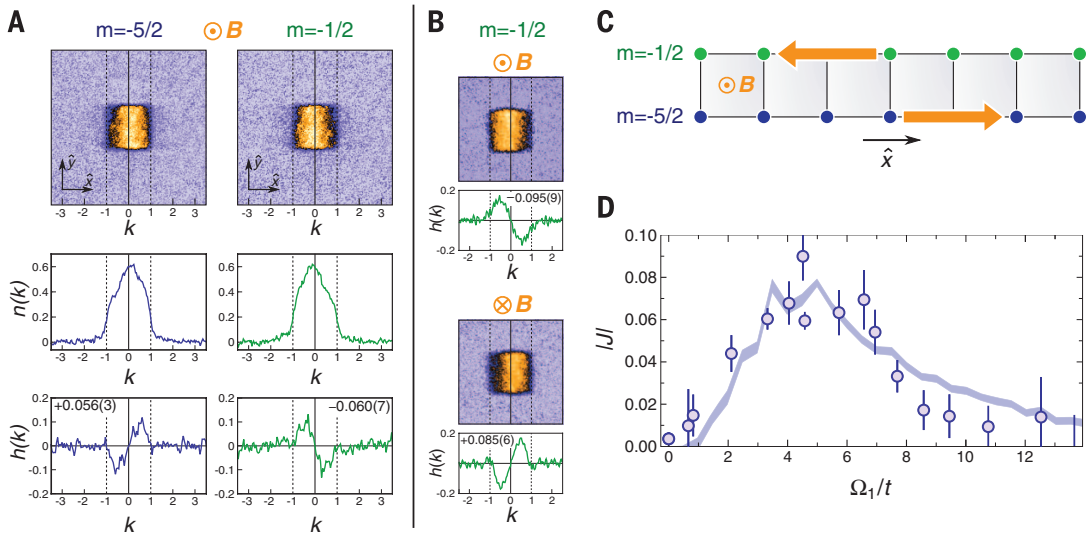

Fig. 2. Chiral dynamics in two-leg ladders. (**A**) (Top) False-color time-of-flight images of the atoms in the $m = -5/2$ and $m = -1/2$ legs (averages of ~30 realizations). (Middle) Integrated lattice momentum distribution $n(k)$. (Bottom) $h(k) = n(k) - n(-k)$ [numerical values within the plots are the net momentum unbalance J determined from $h(k)$]. Experimental parameters: $\Omega_1 = 2\pi \times 489$ Hz, $t = 2\pi \times 134$ Hz, $\Omega_1/t = 3.65$, and $\varphi = 0.37\pi$. (**B**) Time-of-flight images and $h(k)$ of the $m = -1/2$ leg for opposite directions of the effective magnetic field. Experimental parameters: $\Omega_1 = 2\pi \times 394$ Hz, $t = 2\pi \times 87$ Hz, $\Omega_1/t = 4.53$, and $\varphi = \pm 0.37\pi$. (**C**) Sketch of the two-leg ladder configuration realized for this experiment. The arrows are a pictorial representation of the chiral currents. (**D**) Circles show experimental values of $|J|$ for the $m = -1/2$ leg as a function of Ω_1/t (averages of data sets taken for $\varphi = \pm 0.37\pi$). The error bars are obtained with a bootstrapping method applied on ~30 different measurements. The shaded area depicts the result of a numerical simulation that includes thermal fluctuations (*20*).

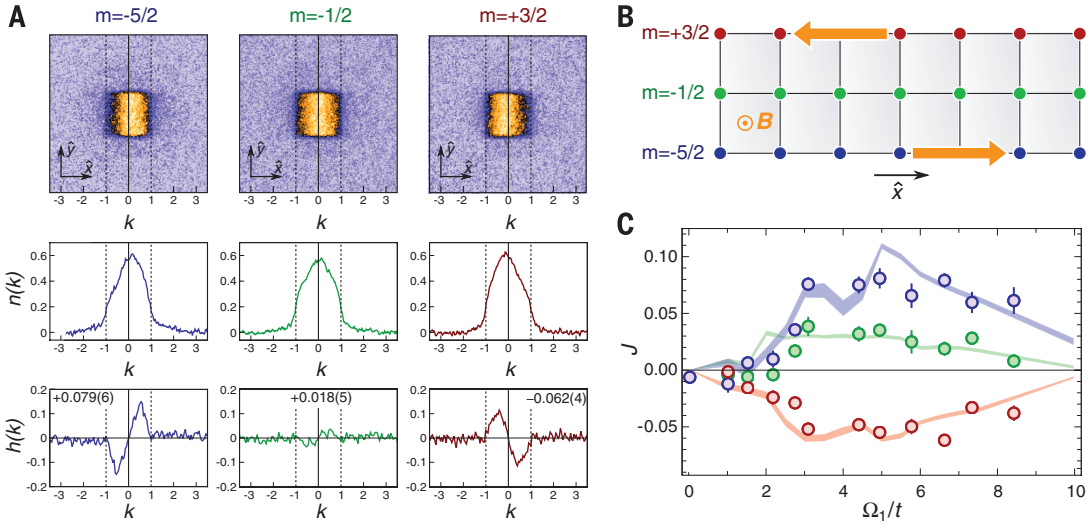

Fig. 3. Chiral edge currents in a three-leg ladder. (**A**) Experimental time-of-flight images (top), $n(k)$ (center), and $h(k) = n(k) - n(-k)$ (bottom) for each of the three legs $m = -5/2$, $m = -1/2$, and $m = +3/2$ constituting the ladder, respectively [numbers shown in the bottom panels are the values of J determined from $h(k)$]. Experimental parameters: $\Omega_1 = 2\pi \times 620$ Hz, $t = 2\pi \times 94$ Hz, $\Omega_1/t = 6.60$, and $\varphi = 0.37\pi$. (**B**) Sketch of the three-leg ladder configuration realized for this experiment. (**C**) Circles show experimental values of the net momentum unbalance J for each leg as a function of Ω_1/t. The shaded areas illustrate the results of a numerical simulation (*20*). For both experimental and simulation data, blue, green, and red correspond to $m = -5/2$, $m = -1/2$, and $m = 3/2$, respectively.

coupling between the legs so as to adiabatically load the fermionic system in the lowest band of both the lattice and the Raman-dressed energy spectrum.

Despite the absence of a real bulk region, this two-leg configuration is expected to support chiral currents with atoms flowing in opposite directions along the legs (Fig. 2C), as investigated recently in bosonic systems (*24*). To observe this, we measured the relative motion of the atoms in the two legs by spin-selective imaging of the lattice momentum distribution, obtained by switching off the synthetic coupling and releasing the atoms from the lattice. In Fig. 2A (upper panel), we show two time-of-flight images corresponding to the $m = -5/2$ and $m = -1/2$ legs (Fig. 2C) for $\Omega_1 = 2\pi \times 489$ Hz and $t = 2\pi \times 134$ Hz ($\Omega_1/t = 3.65$). Here we are interested only in direction $\hat{x}$, which reflects the distribution of the lattice momenta k along the legs (in units of the real-lattice wave number $k_L = \pi/d$, where d is the real-lattice spacing). The lattice momentum distribution along $\hat{y}$ is a uniform square due to the presence of the strong optical lattice along the transverse (frozen) real directions (*20*). The central panel of Fig. 2A shows the lattice momentum distribution $n(k)$ after integration of the images along $\hat{y}$ and normalization according to $\int n(k)dk = 1$. We observe a clear asymmetry in $n(k)$ [similar to what was reported in experiments with spin-orbit coupling in harmonically trapped gases (*25*–*27*)], which we characterize by defining the function

$$h(k) = n(k) - n(-k) \qquad (2)$$

which is plotted in the lower panel of Fig. 2A. The expression $J = \int_0^1 h(k)dk$ provides a measurement of the lattice momentum unbalance and quantifies the strength of the chiral motion of the particles along the two legs. The values $J = +0.056(3)$ for $m = -5/2$ and $J = -0.060(7)$ for $m = -1/2$ are approximately equal in intensity and opposite in sign, providing direct evidence for presence of chirality in the system. The small value of J is attributable to the fact that, in addition to states exhibiting chiral currents, fermions occupy other states at the bottom of the band, which do not display chiral features. We also performed the same experiment with a reversed direction of the synthetic magnetic field **B** (Fig. 2B), observing a change of sign in J, corresponding to currents circulating in the opposite direction. This behavior confirms the interpretation of our data in terms of chiral currents induced by a synthetic magnetic field in a synthetic 2D lattice.

The stability of chiral edge states in fermionic systems is of key importance, for example, for quantum information applications. In our system, the appearance of a chiral behavior is governed by several key parameters, including the ratio Ω_1/t, the Fermi energy E_F, and the flux φ. These parameters are easy to adjust, so they can be used to investigate the rise and fall of the edge currents as a function of the Hamiltonian parameters (*24*), as well as to identify which regimes exhibit stronger chiral features. By varying the tunneling rates along $\hat{x}$ and $\hat{m}$, we observe a phase transition between a chiral behavior and a nonchiral regime. The lattice momentum distribution is measured as a function of Ω_1/t without affecting other relevant parameters, such as E_F and T. Figure 2D illustrates the measurement of $|J|$ as a function of Ω_1/t (circles). As expected, no chirality is observed for vanishing Ω_1, when the legs are decoupled. Chirality is also suppressed for large inter-edge coupling $\Omega_1 \gg t$. In the latter regime, the largest energy scale in the system is the effective kinetic energy along the synthetic direction: This contribution is minimized when the fermions occupy the lowest energy state on each rung, which does not exhibit any chiral behavior. The measured values of $|J|$ compare well with the results of a numerical simulation that includes thermal fluctuations (shaded area in Fig. 2D) (*20*).

We next considered a three-leg ladder, which is the minimal configuration for which chiral currents at the edges can be sharply distinguished from the behavior of the bulk. The experimental procedure is analogous to that employed for the two-leg case, with the Raman parameters adjusted to extend the synthetic coupling to $m = +3/2$, with $\Omega_2 \simeq 1.41\ \Omega_1$ (*20*). Figure 3A shows measured $n(k)$ and $h(k)$ for each of the three legs for $\Omega_1 = 2\pi \times 620$ Hz and $t = 2\pi \times 94$ Hz ($\Omega_1/t = 6.60$). We observe strong chiral currents in the upper- and lower-edge chains, showing values of J with opposite sign, similar to the two-leg case [$J = +0.079(6)$ for $m = -5/2$ and $J = -0.062(4)$ for $m = +3/2$]. In contrast, the central leg shows a much-reduced asymmetry in $n(k)$ [$J = 0.018(5)$], signaling a suppressed net current in the bulk. This is direct evidence of the existence of chiral states propagating along the edges of the system, which leave the bulk mostly decoupled from the edges (Fig. 3C). This behavior is akin to what is expected for a fermionic system in a Harper-Hofstadter Hamiltonian. Bulk states exhibit only local circulations of current, which average to zero when all of the different states enclosed by the Fermi surface are considered. Only the edges of the system experience a nonzero current, because there the chiral nature of the states prevents this cancellation effect from occurring. In the ribbon geometry of the experiment, the bulk reduces to just a single central line. Nevertheless, the behavior discussed above is clearly present and detectable in the experimental signal. The small width of the ribbon favors the observation of edge states, given the large boundary-to-surface ratio of the system, which is reflected in a substantial population of states with edge character.

Figure 3C shows the values of J as a function of Ω_1/t for the three different legs of the ladder. The results illustrate the role of the bulk-edge coupling:

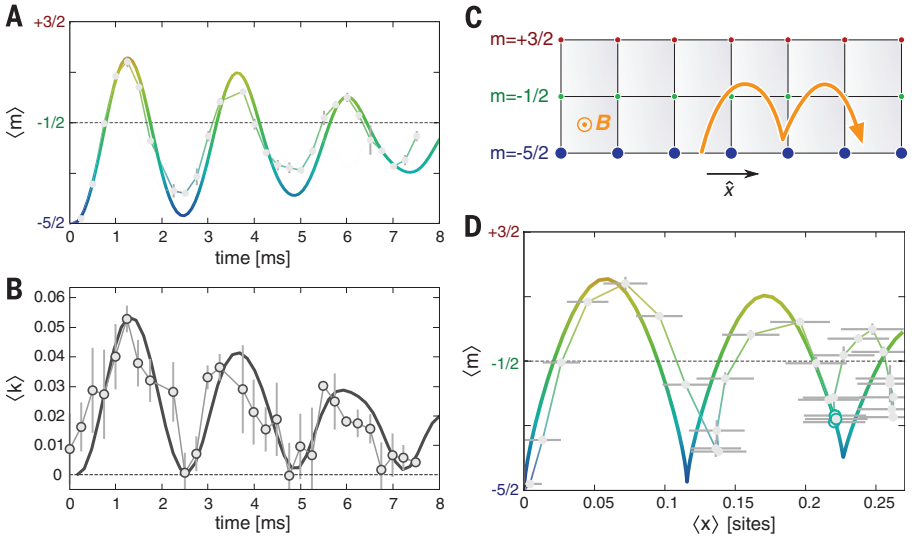

Fig. 4. Edge-cyclotron orbits. (**A**) Time dependence of the average position in the synthetic direction $\langle m \rangle$ after a quench on the synthetic tunneling. (**B**) Time dependence of the average lattice momentum $\langle k \rangle$ along the $\hat{x}$ direction. (**C**) Schematics of the edge-cyclotron orbits. (**D**) Average position in $\hat{m}$–$\hat{x}$ space. The circles in (A), (B), and (D) represent experimental data, the thin lines connect the points, and the thick lines illustrate the theoretical predictions (*20*). Experimental parameters: $\Omega_1 = 2\pi \times 490$ Hz and $t = 2\pi \times 94$ Hz. After the second orbit in (D), the mismatch between theory and experiment could possibly be ascribed to an accumulation of integration error in the data analysis, which amplifies the effects of the assumptions in the model (such as not accounting for interactions).

Similar to the two-leg case, chirality is very weak for small coupling and increases as Ω_1/t approaches ~3. The theoretical curves show that further increasing Ω_1/t eventually leads to attenuation of the signal because of effective coupling between the edges, which smoothens the chiral features of the system. We observe a substantial agreement between experiment and theory for the range of Ω_1/t that can be explored in our experimental setup. The nonzero current in the bulk ($J < 0.035$) can be ascribed to the different couplings (Ω_1 and Ω_2), as well as to a residual light shift that breaks the symmetry between the two edges (*20*).

Finally, we performed additional quench dynamics experiments that provide direct evidence of chiral transport properties along the edges. We prepared a system of lattice fermions in an initial state with zero average momentum on the lower $m = -5/2$ leg of a three-leg ladder. We then performed a quench by suddenly activating the complex tunneling in the synthetic direction. Figure 4A shows the time dependence of the average position in the synthetic direction $\langle m \rangle$, measured by optical Stern Gerlach detection (*23*). Figure 4B shows the time dependence of the average lattice momentum $\langle k \rangle$ along $\hat{x}$, measured by time-of-flight imaging of the whole cloud. Figure 4D shows an experimental reconstruction of the average orbit on the ribbon surface as a plot of $\langle m \rangle$ versus the average position in real space $\langle x \rangle$. The latter has been determined by evaluating the average velocity along $\hat{x}$, considering the knowledge of energy band dispersion versus lattice momentum, and then performing an integration in time (*20*). The dynamics displays a strong chiral character, demonstrated by the in-phase oscillations in Fig. 4, A and B, and the orbits in Fig. 4D. Under the effect of the synthetic magnetic field, the fermions move according to cyclotron-type dynamics, which is naturally truncated by the synthetic edge, giving rise to a skipping-type orbit, as expected for a quantum Hall system (*12*, *13*). Furthermore, the experimental data are in reasonable agreement with the theoretical predictions, represented by the thick lines in Fig. 4, A, B, and D. These dynamics are effectively damped, even in the idealized case described by theory (Fig. 4, A and B), as a result of averaging over many different fermionic trajectories, which also causes a reduction of the average orbit radius to less than one real lattice site (Fig. 4D). This is markedly different from the behavior of a noninteracting Bose gas, which would occupy a single condensed wave packet undergoing undamped oscillations.

Our approach can be extended to wide ladder systems with as many as $2I + 1$ legs, providing a setting for the investigation of both edge and bulk 2D topological matter, complementary to recent works on Chern insulators (*9*). This would allow a controlled study of the combined effect of interactions and synthetic gauge fields, crucial for the realization of fractional quantum Hall physics, potentially leading to exotic states of matter (such as chiral Mott insulator states) in ladder systems. Moreover, the flexibility offered by the present scheme allows the engineering of arbitrary lattice patterns, including disorder and constriction, in ladder systems. This opens the door for the realization of interferometers for chiral liquids, investigation of their transport properties, and the possibility of implementing interfaces between chiral edges, which, in the presence of a molecular or superconducting reservoir (*17*), can potentially host exotic non-Abelian anyons such as Majorana-like states (*16*).

REFERENCES AND NOTES

1. M. Lewenstein, A. Sanpera, V. Ahufinger, *Ultracold Atoms in Optical Lattices: Simulating Quantum Many-Body Systems* (Oxford Univ. Press, Oxford, 2012).
2. I. Bloch, J. Dalibard, S. Nascimbène, *Nat. Phys.* **8**, 267–276 (2012).
3. D. Jaksch, P. Zoller, *New J. Phys.* **5**, 56 (2003).
4. J. Dalibard, F. Gerbier, G. Juzeliūnas, P. Öhberg, *Rev. Mod. Phys.* **83**, 1523–1543 (2011).
5. N. Goldman, G. Juzeliūnas, P. Öhberg, I. B. Spielman, *Rep. Prog. Phys.* **77**, 126401 (2014).
6. Y.-J. Lin, R. L. Compton, K. Jiménez-García, J. V. Porto, I. B. Spielman, *Nature* **462**, 628–632 (2009).
7. M. Aidelsburger *et al.*, *Phys. Rev. Lett.* **111**, 185301 (2013).
8. H. Miyake, G. A. Siviloglou, C. J. Kennedy, W. C. Burton, W. Ketterle, *Phys. Rev. Lett.* **111**, 185302 (2013).
9. G. Jotzu *et al.*, *Nature* **515**, 237–240 (2014).
10. F. D. M. Haldane, *Phys. Rev. Lett.* **61**, 2015–2018 (1988).
11. L. Duca *et al.*, *Science* **347**, 288–292 (2015).
12. X.-G. Wen, *Quantum Field Theory of Many-Body Systems* (Oxford Univ. Press, Oxford, 2004).
13. R. E. Prange, S. M. Girvin, *The Quantum Hall Effect* (Springer, New York, 1990).
14. A. Celi *et al.*, *Phys. Rev. Lett.* **112**, 043001 (2014).
15. N. Y. Yao *et al.*, *Nat. Commun.* **4**, 1585 (2013).
16. C. Nayak, S. H. Simon, A. Stern, M. Freedman, S. Das Sarma, *Rev. Mod. Phys.* **80**, 1083–1159 (2008).
17. N. H. Lindner, E. Berg, G. Refael, A. Stern, *Phys. Rev. X* **2**, 041002 (2012).
18. During the completion of this manuscript, we became aware of a closely related experimental work with Raman-coupled Bose-Einstein condensates (*28*).
19. O. Boada, A. Celi, J. I. Latorre, M. Lewenstein, *Phys. Rev. Lett.* **108**, 133001 (2012).
20. Full details on the experimental and theoretical procedures are available as supplementary materials on *Science* Online.
21. M. A. Cazalilla, A. M. Rey, *Rep. Prog. Phys.* **77**, 124401 (2014).
22. S. Taie, R. Yamazaki, S. Sugawa, Y. Takahashi, *Nat. Phys.* **8**, 825–830 (2012).
23. G. Pagano *et al.*, *Nat. Phys.* **10**, 198–201 (2014).
24. M. Atala *et al.*, *Nat. Phys.* **10**, 588–593 (2014).
25. Y.-J. Lin, K. Jiménez-García, I. B. Spielman, *Nature* **471**, 83–86 (2011).
26. P. Wang *et al.*, *Phys. Rev. Lett.* **109**, 095301 (2012).
27. L. W. Cheuk *et al.*, *Phys. Rev. Lett.* **109**, 095302 (2012).
28. B. K. Stuhl, H.-I Lu, L. M. Aycock, D. Genkina, I. B. Spielman, *Science* **349**, 1514–1518 (2015).

ACKNOWLEDGMENTS

We thank A. Celi and P. Massignan for early stimulating discussions on the synthetic dimension approach. M.D. and M.R. thank C. Laflamme and A. Sterdyniak for discussions. The experimental work in Florence, Italy, was supported by European Union (EU) grant FP7 SIQS, Ministero dell'Istruzione, dell'Università e della Ricerca (MIUR) grant PRIN2012 AQUASIM, and European Research Council (ERC) Advanced Grant DISQUA. The theoretical work in Innsbruck, Austria, was supported by ERC Synergy Grant UQUAM, SFB FoQuS of the Austrian Science Fund, and EU grant FP7 SIQS.

SUPPLEMENTARY MATERIALS

www.sciencemag.org/content/349/6255/1510/suppl/DC1
Supplementary text
Figs. S1 to S4
References (*29*–*32*)

9 February 2015; accepted 28 July 2015
10.1126/science.aaa8736

Observation of chiral edge states with neutral fermions in synthetic Hall ribbons

M. Mancini *et al.*

Science **349**, 1510 (2015);
DOI: 10.1126/science.aaa8736